ELSEVIER

Cell Calcium 43 (2008) 184–195

cell calcium

www.elsevier.com/locate/ceca

Endoplasmic reticulum stress and alteration in calcium homeostasis are involved in cadmium-induced apoptosis

Marta Biagioli [a,*], Simone Pifferi [a,1], Matilde Ragghianti [a], Stefania Bucci [a], Rosario Rizzuto [b], Paolo Pinton [b]

[a] *Laboratory of Cellular and Development Biology, Department of Biology, University of Pisa, Italy*
[b] *Department of Experimental and Diagnostic Medicine, Section of General Pathology and Interdisciplinary Centre for the Study of Inflammation (ICSI), University of Ferrara, Italy*

Received 14 January 2007; received in revised form 30 April 2007; accepted 8 May 2007
Available online 22 June 2007

Abstract

Cadmium, a toxic environmental contaminant, exerts adverse effects on different cellular pathways such as cell proliferation, DNA damage and apoptosis. In particular, the modulation of Ca^{2+} homeostasis seems to have an important role during Cd^{2+} injury, but the precise assessment of Ca^{2+} signalling still remains poorly understood. We used aequorin-based probes specifically directed to intracellular organelles to study Ca^{2+} changes during cadmium injury. We observed that cadmium decreased agonist-evoked endoplasmic reticulum (ER) Ca^{2+} signals and caused a 40% inhibition of sarcoplasmic–ER calcium ATPases activity. Moreover, time course experiments correlate morphological alterations, processing of *xbp-1* mRNA and caspase-12 activation during cadmium administration. Finally, the time response of ER to cadmium injury was compared with that of mitochondria. In conclusion, we highlighted a novel pathway of cadmium-induced cell death triggered by ER stress and involving caspase-12. Mitochondria and ER pathways seemed to share common time courses and a parallel activation of caspase-12 and caspase-9 seemed likely to be involved in acute cadmium toxicity.

Keywords: Cadmium; Aequorin chimeras; Endoplasmic reticulum; Calcium homeostasis; Sarcoplasmic–endoplasmic reticulum calcium ATPases; Apoptosis; Caspases

1. Introduction

We analysed the mechanisms of cellular toxicity associated to cadmium exposure. This heavy metal, widely diffused in the ecosystems because of its large use in different kinds of industries and other human activities, is characterized by a very long half life [1,2]. Chronic exposure to cadmium in humans is associated with bone, lung and renal damage. Furthermore, evidences of human carcinogenicity are also available linking long-term occupational exposure to increased occurrence of lung, prostate and renal cancer cases [3,4].

At the cellular level, cadmium has been also associated with different biochemical changes characteristic of programmed cell death (PCD) [5].

Even if several hypotheses have been proposed, the mechanisms for cadmium-induced apoptosis remain poorly understood. Alteration in calcium homeostasis and mitochondrial damage [6,7] have been involved with cadmium-induced apoptosis, but other intracellular targets could not be ruled out.

Calcium is a ubiquitous intracellular signal responsible for controlling numerous cellular processes including proliferation, differentiation, development and cell death [8,9]. Thus, it is not surprising that changes in Ca^{2+} concentration

* Corresponding author. Present address: Laboratory of Molecular Neurobiology, International School for Advanced Studies (ISAS), Area Science Park Basovizza Building Q1, SS 14 Km 163,5, 34012 Trieste, Italy.
Tel.: +39 040 3756535; fax: +39 040 3756502.
E-mail address: biagioli@sissa.it (M. Biagioli).
[1] Present address: Neurobiology Sector, International School for Advanced Studies (ISAS), Trieste, Italy.

0143-4160/$ – see front matter © 2007 Elsevier Ltd. All rights reserved.
doi:10.1016/j.ceca.2007.05.003

in cytoplasm as well as in different intracellular organelles could be responsible for induction of apoptosis [10]. Cadmium is reported to interfere with cell calcium homeostasis at different levels. The similarity between hydrated radius of Cd^{2+} and Ca^{2+} ions [11] is the first way to explain the inhibition, observed upon cadmium treatment, of receptor and voltage operated calcium channels as well as all types of Ca^{2+}-APTases pumps [12–19]. Moreover, cadmium is also able to induce a rapid transient of cytosolic calcium by stimulating receptor-mediated mobilization from intracellular calcium stores [20].

Even if the interference of cadmium with the regulation of Ca^{2+} homeostasis has been studied previously, the pertinent mechanisms of this interference are not elucidated satisfactorily. A major problem in the interpretation of the results originated from the use of fluorescent indicators (such as Fura-2). Fura-2 binds cadmium and other divalent ions with very high affinity [21]; therefore, it has been difficult to distinguish between calcium and cadmium signals.

In this report, we measured cadmium-induced alteration on intracellular calcium homeostasis by the use of modified targeted chimeras of Ca^{2+} sensitive photo protein aequorin. We investigate, in fact, the differential effects on calcium signalling during cadmium injury in specific subcellular organelles and compartments.

Numerous pro-apoptotic signals and damage pathways converge on mitochondrial membranes to induce their permeabilization [22]. Mitochondrial membrane permeabilization (MMP) triggers the release of proteins that are normally strictly confined to the mitochondrial intermembrane space, in particular cytC (which stimulates the cytosolic assembly of the apoptosome, the caspase-9 activation complex) and AIF (apoptosis-inducing factor) [23]. Finally, the activation of catabolic hydrolases, mainly caspases and nucleases, causes the cleavage of important cellular targets and leads to apoptotic cell death.

Some evidences came in the last years about the ability of cadmium to directly [7] or indirectly [6] induce MMP. Moreover, acute cadmium treatment seems to be correlated with reduction in cellular redox potential and with reactive oxygen species formation in C6 cells [24] and in human hepatoma cell line [25]. As a consequence, the mitochondrial potential collapses and caspase-9 is activated [26].

On the other hand, the ER serves many specialized functions in the cell including calcium storage, biosynthesis of membrane and secretory proteins, production of phospholipids and sterols. Disturbance of any of these functions can lead to the so-called ER stress [27]. One of the most characterized and highly conserved ER stress responses is the unfolded-protein response (UPR) [23]. Major cross talks exist between UPR and Ca^{2+} imbalance: Ca^{2+}-depletion or alteration in Ca^{2+} transport systems (SERCAs) can directly cause UPR [10,28]. In turn, if ER stress is prolonged in time and ER resident chaperones are unable to counteract the accumulation of misfolded proteins, an ER mediated apoptotic program is triggered through the activation of caspase-12 [29,30].

In mammalian cells, the UPR seems to be driven by three ER-located transmembrane proteins, ATF-6, IRE1 and PERK. In particular, IRE1 is both a kinase and endoribonuclease. This protein appears to function as sensor of accumulation of unfolded proteins and, upon autophosphorylation, IRE1 initiates the specific spliceosome-independent processing of *xbp-1* mRNA [31,32,33]. Processing of *xbp-1* mRNA results in a translation frame shift that allows encoding of active *xbp-1*, a leucine-zipper transcription factor that can bind ER stress response element and activate the transcription of a set of ER chaperones such as Bip, GADD153/CHOP [33]. In this study, we showed *xbp-1* mRNA processing and the activation of caspase-12 following cadmium treatment demonstrating the induction of ER stress and, subsequently, an ER regulated apoptotic pathway.

In conclusion, our observations, on one hand confirmed previous reports about mitochondrial involvement in cadmium toxicity, but, on the other hand, they led to the discovery of a new intracellular target of cadmium injury—the ER. Moreover, both organelles showed a pronounced alteration in calcium homeostasis and very similar pathways of caspases activation.

2. Methods

2.1. Cell culture and treatment

NIH 3T3 cells (American Tissue Culture Collection) were cultured using Dulbecco's modified Eagle's medium (DMEM; Invitrogen) with 100 U/ml penicillin, 100 μg/ml streptomycin (Invitrogen) and 10% fetal bovine serum (FBS; Invitrogen), at 37 °C in humidified atmosphere of 5% CO_2. Cultures were passaged twice a week.

2.2. Antibodies and reagents

$CdCl_2$, MTT (3-(4,5-dimethylthiazol-2-yl)-2,5-diphenyltetrazolium bromide) and anti-β-actin monoclonal antibody were purchased from Sigma. Anti-caspase-12 monoclonal antibody (SIGMA) was kindly provided by Dr. Mercedes Garcia (University of Pisa). Anti-CytC polyclonal antibody was from BD Bioscience and anti-VDAC (Voltage Dependent Anion Channel) was from Calbiochem.

2.3. Protein extraction, SDS electrophoresis and Western blotting

Cells from different treatment groups were harvested and cell pellets were resuspended in lysis buffer: 1% TRITON-X100, 10% glycerol, 20 mM Tris pH 7.5; 150 mM NaCl, 10 mM EDTA, 1 μg/μl leupeptin, 1 μg/μl aprotinin, 1 mM PMSF. Cellular suspensions, from all the experiments were frozen and thawed three times, maintained 30 min on ice, and then centrifuged at 15,000 × *g* for 30 min at 4 °C. The result-

ing supernatants were collected and protein concentrations were determined by the Bradford assay [34], with bovine serum albumin as calibration standard. Loading buffer was added to each protein sample, which was subsequently boiled for 5 min. Equal amount of proteins were electrophoresed on an SDS-polyacrylamide gel (SDS-PAGE). After SDS-PAGE, proteins were blotted onto immobilon-P PVDF (Polyvinylidene Fluoride) microporous membrane (Millipore). Membranes were blocked in PBS and 0.1% Tween-20 (PTw) +5% dried milk. Membranes were incubated overnight at 4 °C in primary antibody and for 2 h at room temperature with secondary antibody. After washing, protein bands were detected by HRP/hydrogen peroxide catalysed oxidation of luminol by an enhanced chemioluminescence system (PIERCE) and autoradiography.

2.4. Mitochondria preparation

For mitochondria preparation, we basically used the protocol described by Yang et al. [35]. Briefly, the cells were harvested by centrifugation and washed twice in ice-cold PBS. The cell pellet was resuspended in five volumes of buffer A (20 mM Hepes–KOH, pH 7.5, 10 mM KCl, 1.5 mM $MgCl_2$, 1 mM sodium EDTA, 1 mM sodium EGTA, 1 mM dithioerytrol, 250 mM sucrose). Proteases inhibitors were added to buffer A. The cells were homogenized with 30 strokes in a Dounce homogenizer on ice and than centrifuged at 750 g at 4 °C for 10 min. The supernatant was collected and centrifuged again at 10,000 × *g* at 4 °C for 15 min. The resulting mitochondria pellet was dissolved in buffer A and the supernatant was collected to get the cytosolic fraction. Mitochondrial and cytosolic fracstions were used for Western Blotting experiments.

2.5. Densitometric analysis

The bands on the developed film were quantified by Image J (NIH Image, version 1.240) program. The density of each band was normalized to that of a reference protein (β-actin or VDAC).

2.6. Aequorin experiments

For aequorin measurements, NIH 3T3 cells were seeded onto 13 mm cover slips (BDH) previously coated with poly-D-lysine (1 μg/ml in PBS) and transfected with 0.8 μg of aequorin chimeras cDNA using Lipofectamine 2000 reagent (Invitrogen). We used aequorin probes targeted to ER (ER-AEQ) and mitochondria (mtAEQmut) [36].

For mtAEQmut, 36 h post transfection, the coverslips were incubated for 2 h in KRB (Krebs–Ringer modified buffer: 125 mM NaCl, 5 mM KCl, 1 mM Na_3PO_4, 1 mM $MgSO_4$, 5.5 mM glucose, and 20 mM Hepes, pH 7.4) at 37 °C supplemented with coelenterazine (5 μM) and then transferred to the perfusion chamber.

For reconstituting with high efficiency, the AEQ chimeras targeted to the ER, the luminal [Ca^{2+}] of this compartment was first reduced. This was obtained by incubating the coverslips for 1 h at 4 °C in KRB, supplemented with coelenterazine n (5 μM), the Ca^{2+} ionophore ionomycin, and 600 μM EGTA [37,38,39]. After this incubation, the cells were extensively washed with KRB supplemented with 2% BSA and 1 mM EGTA, and then the coverslips were transferred to the perfusion chamber.

All aequorin experiments were carried out 36 h post transfection at 37 °C and the buffer used was KBR, supplemented with either 1 mM $CaCl_2$ or 100 μM EGTA. The agonist bradykinin (Bk) was added to the same medium (see figure legends).

In experiments with digitonin (100 μM) permeabilized cells, using ER-AEQ for the study of SERCA activity, a buffer mimicking the cytosolic ionic composition (intracellular buffer, IB: 140 mM KCl, 10 mM NaCl, 1 mM K_3PO_4, 5.5 mM glucose, 2 mM $MgSO_4$, 1 mM ATP, 2 mM sodium succinate, 20 mM Hepes, pH 7.05, at 37 °C) was employed. The medium was switched from IB with 2 mM EGTA to IB containing contaminant (2 μM) [Ca^{2+}] + ATP and $MgSO_4$, essential cofactors of SERCA pumps.

All the experiments with aequorin were terminated by lysing the cells with 100 μM digitonin in a hypotonic Ca^{2+}-rich solution (10 mM $CaCl_2$ in H_2O), thus discharging the remaining AEQ pool. The light signals were collected and converted into [Ca^{2+}] values after calibration as previously described [36].

2.7. Confocal microscopy analysis

NIH 3T3 cells were seeded onto 24 mm coverslips and transfected with mt-GFP and ER-GFP [40] by using Lipofectamine 2000 (Invitrogen). 24 h post transfection cells were treated with different cadmium concentrations for different times. The treatments were stopped by fixing the cells in 4% paraformaldeyde for 5 min. Fluorescence images were captured by confocal fluorescent microscopy (model LSM 510; Carl Zeiss MicroImaging, Inc.).

2.8. RT-PCR experiments

Total RNA from NIH 3T3 cells was isolated by using Tri Reagent (Sigma). After DNase I treatment, 2 μg of total RNA were retrotranscribed using oligo$(dT)_{15–18}$ (Invitrogen) and SuperScript™ Reverse Transcriptase (Invitrogen). About 3 μl of cDNA were used for PCR amplification using RED-Taq TM PCR reaction Mix (Sigma). The following primers were used in this work:

- *xbp-1* sense: 5′-AAACAGAGTAGCAGCGCAGACTGC-3′.
- *xbp-1* reverse: 5′-GGATCTCTAAAACTAGAGGCTTG-GTG-3′.

- β-actin sense: 5′-CTACCTCATGAAGATCCTCAC-3′.
- β-actin reverse: 5′-TTCGTGGATGCCACAGGACTC-3′.

Equal aliquots of PCR products were electrophoresed through a 2% agarose gel and the bands were revealed by ethidium bromide staining.

2.9. Statistical analysis

Results obtained from at least three different experiments were analysed using Student's *t*-test and they were considered statistically significant at $p < 0.05$. Where various experimental groups were compared to one control group, the statistical analysis was adjusted for multiple comparisons using Benjamini and Hochberg correction. All data reported in this work are the means ± standard error (S.E.).

3. Results

3.1. Calcium homeostasis is affected by cadmium treatment: aequorin measurements

To directly investigate the role of cadmium in Ca^{2+} homeostasis, we selectively measured the $[Ca^{2+}]$ in three different cell compartments, such as cytoplasm, mitochondria and ER. The influence of cadmium on changes in the intracellular Ca^{2+} concentration elicited during stimulation by bradykinin (Bk) was investigated. The hormone Bk mediates Ca^{2+} mobilization by binding to surface receptors. Murine fibroblasts NIH 3T3 have been show to possess this kind of receptors and to be sensitive to Bk stimulation [41]. Bk evokes a Ca^{2+} signal mainly due to the generation of inositol-1,4,5-trisphosphate, which in turn causes a release of Ca^{2+} from internal stores. We have reported previously, that in NIH 3T3 cells transfected with cytosolic aequorin (cyt-AEQ), stimulation by Bk

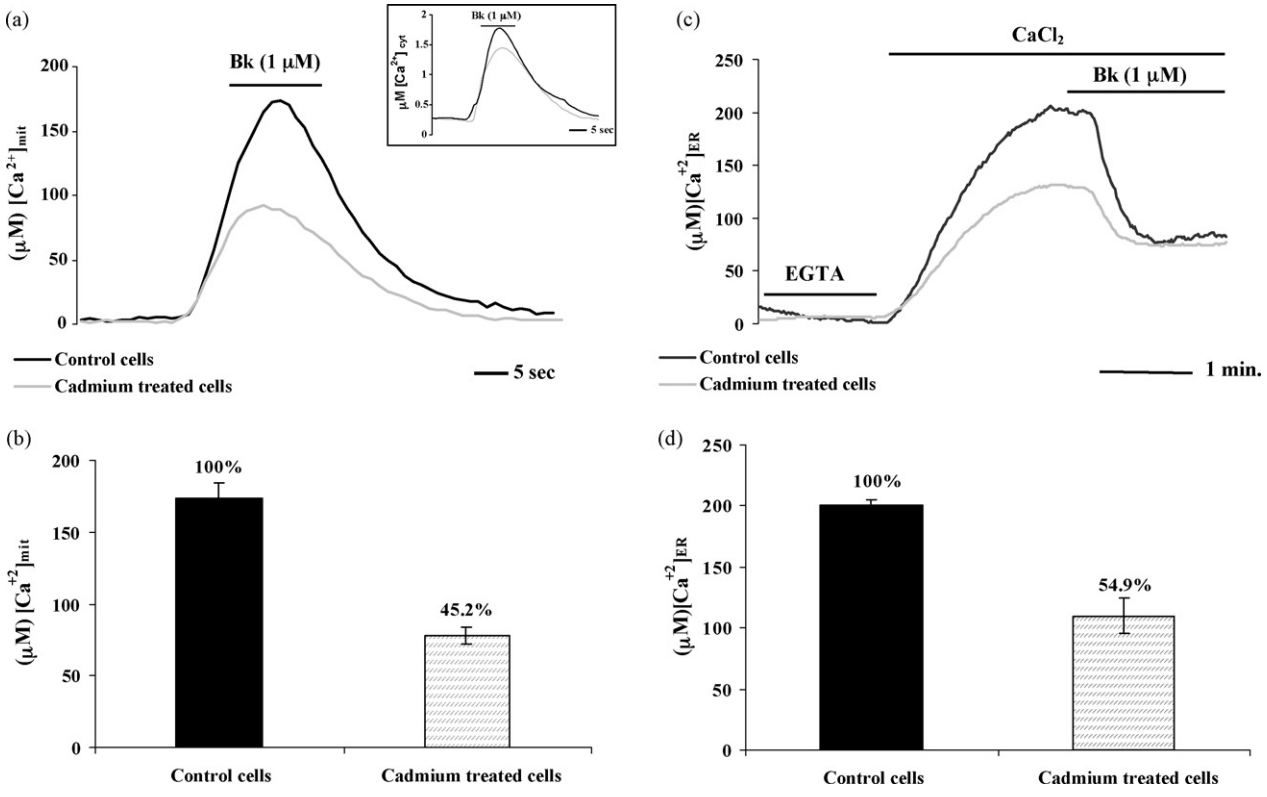

Fig. 1. (a and b) Mitochondrial $[Ca^{2+}]_{mit}$ in control and cadmium treated cells (15 μM for 12 h). mtAEQmut was transfected into NIH 3T3 cells and 36 h later, the measurement of AEQ luminescence was carried out and calibrated into $[Ca^{2+}]$ values. Where indicated, the cells, perfused with KRB, were challenged with 1 μM Bk added to the same buffer. As for cytosol (inset figure) [42], Bk stimulation caused a rapid increase in $[Ca^{2+}]_{mit}$ reaching in control cells a value up to 173.1 ± 10.5 μM ($n = 10$). In cadmium treated cells (12 h) $[Ca^{2+}]_{mit}$ was reduced of 54.8% ($P < 0.01$) and the average value of $[Ca^{2+}]_{mit}$, following Bk stimulation, became 78.2 ± 5.9 μM ($n = 6$). Inset figure shows the kinetics of Ca^{2+} homeostasis in the cytosol upon cadmium treatment for 12 h. Control and cadmium-treated traces use the same colours used for mitochondria. (c and d) $[Ca^{2+}]_{ER}$ in control and cadmium treated cells (15 μM for 12 h). ER-AEQ was transfected into NIH 3T3 and 36 h later, the organelle was depleted of Ca^{2+} to optimise AEQ reconstitution. After reconstitution cells were transferred to the luminometer chamber and AEQ luminescence was collected and calibrated in Ca^{2+} values. In the first part of the experiments, the perfusion medium was switched from KRB + EGTA (1 mM) to KRB + 1 mM $CaCl_2$. In these conditions, $[Ca^{2+}]_{ER}$ gradually increased, reaching in control cells a plateau value of 200.0 ± 5.5 μM ($n = 20$). The refilling of ER Ca^{+2} was sensibly (45%; $P < 0.01$) lowered in Cd^{2+}-treated cells for 12 h and the plateau value was 109.8 ± 14.1 μM ($n = 11$). Where indicated, the cells were stimulated with Bk (1 μM). Bk stimulation caused a rapid release of Ca^{2+} from ER in control cells, however, due to the reduced refilling state, Bk-induced depletion of $[Ca^{2+}]_{ER}$ is larger and faster in control cells as compared to Cd^{2+}-treated cells.

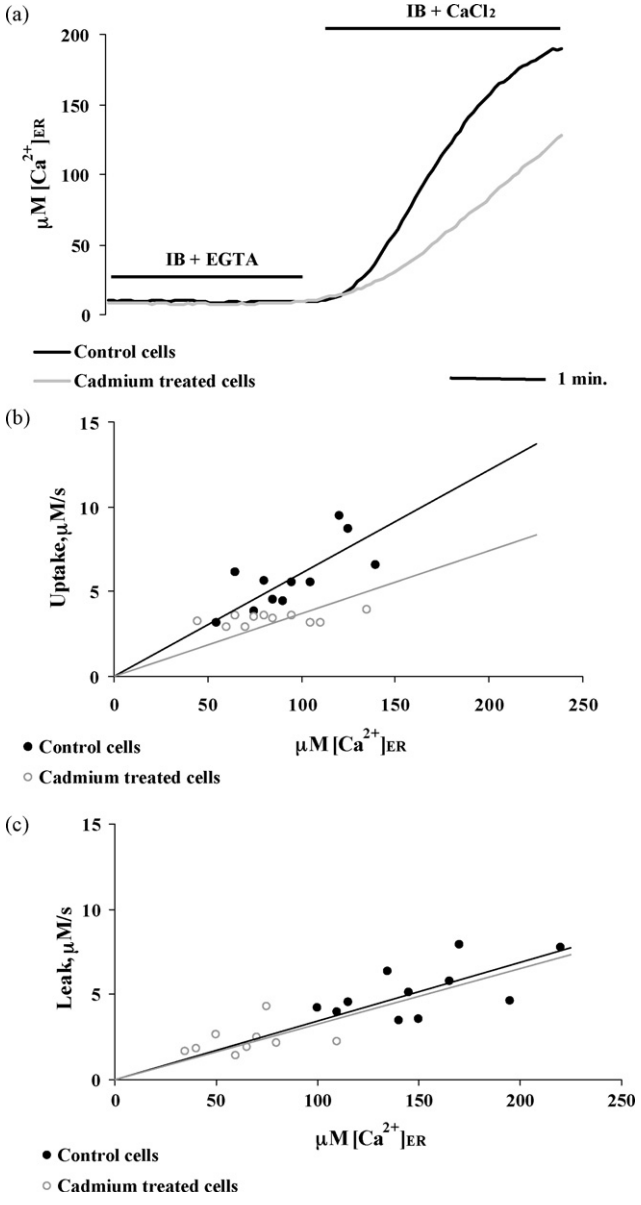

Fig. 2. (a) Kinetics of ER Ca^{2+} uptake in control and Cd^{2+}-treated cells (15 μM for 12 h). NIH 3T3 fibroblasts were transfected with ER-AEQ. AEQ measurements were carried out as in Fig. 1c except that the cells were permeabilized with 100 μM digitonin for 1 min. In these experiments a buffer mimicking intracellular ionic conditions (IB) was used. Ca^{2+} accumulation in the ER was initiated by switching the medium from IB + EGTA to IB containing contaminant $[Ca^{2+}]$ of about 2 μM. The kinetics of ER refilling are reported in the graph. AEQ calibration was carried out as described in Materials and Methods. (b) SERCAs activity in control and Cd^{2+}-treated cells (15 μM for 12 h). Transfection, depletion of Ca^{2+} stores and AEQ reconstitution were carried out as in (a), then the coverslip with the cells was transferred to the luminometer and perfused with IB/Ca^{2+} until the steady-state $[Ca^{2+}]_{ER}$ was reached. Based on the experimental traces (a), the maximal rates of Ca^{2+} uptake (measured from the first derivative) at different values of $[Ca^{2+}]_{ER}$ were calculated and plotted for Cd^{2+}-treated (15 μM for 12 h) and control cells. The plot contains data obtained from 11 independent experiments. Due to the mixing time in the luminometer chamber, the kinetics of $[Ca^{2+}]_{ER}$ uptakes were sigmoidal and the maximal rate was obtained during the first 2–3 s after the beginning of $[Ca^{2+}]_{ER}$ increase. Accordingly, we considered the maximal rates the best approximation for the initial rate of $[Ca^{2+}]_{ER}$ increase. The fitting of the curve shown in this figure was performed using Microsoft Excel software. As revealed by the graphic, the maximal rate of Ca^{2+} uptake was significantly ($P < 0.01$) lowered by cadmium treatment, reaching an average value of 3.4 ± 0.1 μM/s, nearly 40% less than the value obtained in control cells. (c) Ca^{2+} leak rate from ER in control and cadmium-treated cells (15 μM for 12 h) Transfection, depletion of Ca^{2+} stores and AEQ reconstitution were carried out as in Fig. 1c, then the coverslip with the cells was transferred to the luminometer and perfused with KRB/Ca^{2+} until the steady-state $[Ca^{2+}]_{ER}$ was reached. Ca^{2+} release was initiated by treating the cells with 50 μM tBuBHQ, a specific inhibitor of SERCAs pumps. In analogy of that presented on (b), about the rate of Ca^{2+} uptake in ER, based on the experimental traces, the maximal rates of Ca^{2+} release (measured from the first derivative) at different values of $[Ca^{2+}]_{ER}$ were calculated and plotted for Cd^{2+}-treated and control cells. The plot contains data obtained from 9 (cadmium) and 11 (control) independent experiments. Due to the mixing time in the luminometer chamber, the kinetics of $[Ca^{2+}]_{ER}$ decrease are sigmoidal and the maximal rate is obtained 2–3 s after addition of tBuBHQ. Accordingly, we considered the maximal rates the best approximation for the initial rate of $[Ca^{2+}]_{ER}$ decrease. The fitting of the curve shown in this figure was performed using Microsoft Excel software.

(1 μM) evokes a rapid Ca^{2+} transient, reaching a peak value of about 2.3 ± 0.1 μM and that cadmium (15 μM) administered for 12 h causes a nearly 25% reduction of Ca^{2+} elevation during Bk stimulation (Fig. 1a, inset) [42]. The same conditions, i.e. cadmium treatment and mode of Bk stimulation were employed also for the experiments presented here.

A result similar to that reported for the cytosol was found in mitochondria using mitochondria-targeted aequorin (mtAEQmut) (Fig. 1a). In fibroblasts treated with 15 μM cadmium for 12 h, the $[Ca^{2+}]_{mit}$ spike evoked by Bk stimulation decreased from 173.1 ± 10.5 μM in control cells to 78.2 ± 5.9 μM, i.e. by 55%. As expected, given the non-linear dependence of mitochondrial Ca^{2+} accumulation on $[Ca^{2+}]_{cyt}$ [43], the mitochondrial Ca^{2+} response follows and amplifies the cadmium-dependent reduction in agonist-dependent cytosolic rise.

The most interesting situation was found in the ER. In this case, as the ER has a very high Ca^{2+} concentration it was necessary to lower the lumenal Ca^{2+} concentration before adding the prosthetic group to achieve the reconstitution of active aequorin. To this end, the cells were preincubated with ionomycin and a Ca^{2+} chelating agent (EGTA). After reconstitution, the concentration of free Ca^{2+} was <10 μM into this organelle. When the Ca^{2+} concentration in the perfusion medium was raised to 1 mM, the Ca^{2+} concentration in the lumen gradually increased, reaching a plateau value of 200.0 ± 5.5 μM (control cells) (Fig. 1c).

In the control cells, stimulation with Bk caused a large, rapid fall in the ER Ca^{2+} concentration down to a value of approximately 60–70 μM. In cells treated with 15 μM cadmium for 12 h (Fig. 2a) the refilling of ER Ca^{2+} is considerably lowered to 109.8 ± 14.1 μM, i.e. 45%, as compared to control cells. This depletion of ER Ca^{2+} stores is responsible for the strong reduction in Bk mediated $[Ca^{2+}]$ peak in the cytosol and in mitochondria.

3.2. Mechanisms of cadmium-induced $[Ca^{2+}]_{ER}$ alteration

Given that the steady-state $[Ca^{2+}]$ in ER depends on the equilibrium between active accumulation and passive leakage, cadmium could affect either process. Cd^{2+} could reduce Ca^{2+} uptake by the SERCAs, either by a direct effect on the pumps or by reducing the resting cytosolic $[Ca^{2+}]$. On the other hand, it could increase the passive leak of Ca^{2+} from the ER. To clarify these two hypotheses, we investigated them independently.

We investigated whether cadmium treatment had any direct effect on the activity of the SERCA pumps. For this purpose, the kinetics of Ca^{2+} accumulation were studied in permeabilized cells in order to avoid other side effects of this cation (Fig. 2a and b). After reconstituting the photoprotein as in the experiment of Fig. 1c, cadmium-treated and control cells were transferred to the luminometer chamber and perfused with IB/EGTA, a buffer mimicking intracellular ionic conditions, supplemented with 100 μM EGTA. After permeabilization with 100 μM digitonin and washing with IB/EGTA, the medium was switched to IB, containing only a contaminant Ca^{2+} concentration (about 2 μM) (IB/Ca^{2+}). Under those conditions, $[Ca^{2+}]_{ER}$ gradually increased, reaching a plateau value of 193.9 ± 11.1 μM. In cadmium-exposed cells the steady state Ca^{2+} concentration was lower (155.8 ± 6.2 μM). Moreover, in cadmium–treated cells, the maximal rate of Ca^{2+} accumulation was considerably reduced in comparison to control cells from 5.9 ± 0.5 to 3.4 ± 0.1 μM/s, i.e. to 42.8% (Fig. 2b) arguing that the Ca^{2+} uptake activity is modified during cadmium exposure. Moreover, in agreement with the above results, a clear difference in the ER Ca^{2+} uptake was present also in intact cells as shown in Fig. 1c.

To test whether cadmium really inhibits the Ca^{2+} uptake activity and does not enhance the leak rate from the ER, cadmium-treated and control cells, were prepared as described for the experiment of Fig. 1c. After the depletion protocol, the ER of control and cadmium-treated cells was first refilled by exposing the cells to 1 mM extracellular Ca^{2+}, thus resulting in different levels of steady state $[Ca^{2+}]_{ER}$. A SERCA blocker, 2,5-di-(*tert*-butyl)-1,4-benzohydroquinone (tBuBHQ), was then added to initiate the release of stored Ca^{2+}. Given that, by definition, the rates of Ca^{2+} uptake and leak in the steady state are equal, the rate of $[Ca^{2+}]_{ER}$ decrease upon blockade of the SERCA must reflect the rate of Ca^{2+} cycling across the ER membrane and, thus the leak rate at any given steady state of $[Ca^{2+}]_{ER}$ [44]. Fig. 2c shows the relationship between different $[Ca^{2+}]_{ER}$ values and the maximum rates of Ca^{2+} release calculated from the first derivative for cadmium-treated and control cells. As clearly visible form the fitting curve obtained using Microsoft's Excel software, the rate of Ca^{2+} efflux is rather the same in cadmium treated and control fibroblasts, suggesting that the Ca^{2+} leak rate from ER is not affected by cadmium.

3.3. Mitochondrial and endoplasmic reticulum morphology

We investigated whether the $[Ca^{2+}]_{mit}$ and $[Ca^{2+}]_{ER}$ changes were paralleled by alterations of organelle morphology compatible with the onset of apoptosis. By means of mitochondria and ER-targeted GFP chimeras, we were able to follow the modification of mitochondria and ER during cadmium exposure. NIH 3T3 cells were transfected with mt- or ER-GFP and the effects of cadmium on the structures of mitochondria and ER were evaluated. We followed the morphology of these organelles after the administration of 15 or 30 μM $CdCl_2$ for different times (3, 6, 9, and 12 h).

About 15 μM $CdCl_2$ was a previously described concentration able to induce 50% drop in viability and induction of apoptosis after 24 h of treatment [42]. This concentration, however, was only moderately toxic after 12 h of treatment: MTT assays revealed a tendency in reduction in viability of about 10–15% (data not shown). The higher concentration of 30 μM $CdCl_2$ induced a drop in viability of nearly 60% after only 12 h of treatment. In each experimental group at least three different architectures of mitochondria and ER could be described. In Fig. 3 the typical mitochondrial network characteristic of cells in physiologic conditions could be appreciated. This morphology is defined as *normal*. Conversely, mild alterations in mitochondrial morphology started to be visible in Fig. 3b, defining a *mild* phenotype. A more severe rupture and fragmentation of mitochondrial network, characterized by condensation into amorphous dense masses, could be easily appreciated in Fig. 3c and is defined as *strong* phenotype.

As for mitochondria, ER-targeted GFP was transfected into NIH 3T3 cells and organelle structure was evaluated in control cells and Cd^{2+} exposed fibroblasts (15–30 μM $CdCl_2$ for 3, 6, 9 and 12 h). In a similar way as for mitochondria, we described *normal*, *mild* and *strong* ER morphologies. In Fig. 4a the ER network of interconnected closed vesicles, characteristic of control cells, could be appreciated. Conversely, a drastic alteration of ER morphology was already visible in Fig. 4b describing a *mild* phenotype. Even if in this picture the collapse of ER structure start to be clear in various regions of the cell, the *strong* disruption of ER became clear in Fig. 4c as a complete condensation of ER, falling down around the nucleus.

The number of cells, bearing a specific ER or mitochondria morphology, was counted for control and cadmium-treated cells. The results for mitochondria were presented in Table 1. Using the concentration of 15 μM $CdCl_2$, we could observe a significant increase in mitochondrial damage, expressed as number of cells with *mild* or *strong* phenotype, after 9 and 12 h of treatment. Nearly the same results were obtained analysing ER morphology: a parallel disruption of ER structure was observed at 9 and 12 h of cadmium treatment (Table 2). The use of a stronger cadmium concentration (30 μM) enabled us to observe an earlier and

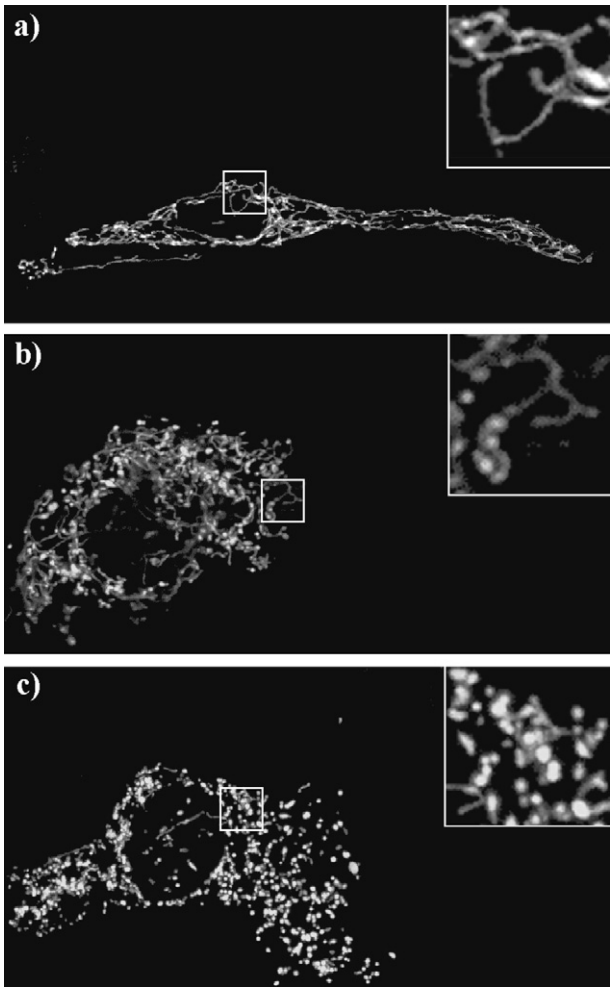

Fig. 3. Cadmium-induced morphological changes in the mitochondrial network. Mitochondrial structure was evaluated by visualizing mt-GFP with a confocal microscope. After transfection, the cells were treated with 15 or 30 μM cadmium and they were fixed after different times treatment (0, 3, 6, 9 and 12 h). In each treatment group three different types of mitochondrial morphology are distinguished: (a) *normal* morphology characterized by an interconnected and continuous mitochondrial network; (b) *mild* disruption structure, visible as condensation of the mitochondrial network; (c) *strong* disruption of the mitochondria which appear completely condensed and fragmented. In each picture a square region has been magnified in order to better appreciated the fine architecture of mitochondria.

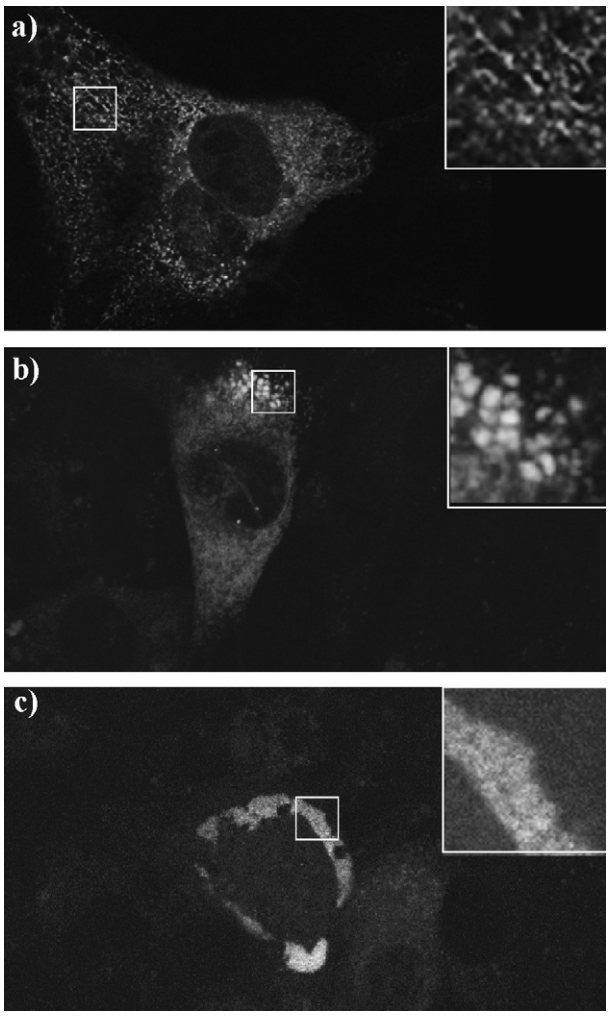

Fig. 4. Cadmium-induced morphological changes in the ER structure. ER structure was evaluated by visualizing ER-GFP with a confocal microscope. After transfection, the cells were treated with 15 or 30 μM cadmium and they were fixed after different times treatment (0, 3, 6, 9 and 12 h). In each treatment group we could distinguish at least three different types of ER morphology: (a) *normal* morphology characterized by the fine ER network; (b) *mild* disruption structure, where the collapse of ER structure starts to be clear in various regions of the cell; (c) *strong* disruption of ER which appear as a complete condensation of ER which fall down around the nucleus. In each picture a square region has been magnified in order to better appreciated the fine architecture of ER.

severer disturbance of ER and mitochondrial morphology. Also in this case, however, the time course analysis demonstrated a nearly complete similarity in the temporal patterns of ER and mitochondria morphology, showing a significant disruption of the networks after only 3 h of cadmium treatment.

3.4. Cadmium-induced ER stress

To study if cadmium-treatment may cause ER stress, thus mediating apoptosis via ER, we analysed two different parameters, following described.

3.4.1. Activation of unfolded protein response (UPR) during cadmium treatment

Upon activation of the UPR, *xbp-1* mRNA is cleaved by the IRE1 protein to remove a 26-nucleotide intron and generate a translational frame shift. The resulting processed mRNA encodes a protein with a novel C-terminus that acts as a potent transcriptional activator. In order to demonstrated if cadmium was able to induce ER stress and UPR, we analysed the splicing of *xbp-1* mRNA by RT-PCR. We demonstrated that cadmium exposure induced the splicing of *xbp-1* mRNA in NIH 3T3 mouse fibroblasts in a time and dose dependent manner as observed in Fig. 5 where the 575 bp (Fig. 5 asterisk)

Table 1
Mitochondrial morphology upon cadmium treatment

	15 μM cadmium treatment (h)				
	0	3	6	9	12
Mitochondrial morphology description					
Normal	94 ± 5.2	95.7 ± 4.8	86.7 ± 10.4	72.3 ± 7.7	71.7 ± 11.7
Mild	4.3 ± 4.6	3.3 ± 4.8	11.7 ± 9.3	21.3 ± 4.4	19 ± 8.3
Strong	1.7 ± 1.6	1 ± 0	1.7 ± 1.7	6.4 ± 4.8	9.3 ± 4
	30 μM cadmium treatment (h)				
	0	3	6	9	12
Mitochondrial morphology description					
Normal	96.5 ± 2.3	93 ± 4	75.3 ± 7.6	62.2 ± 4.3	52.5 ± 4.6
Mild	2.17 ± 1.3	6 ± 2.08	18.5 ± 5	31.1 ± 4.2	36.5 ± 2.1
Strong	1.33 ± 1.3	1 ± 2	6.17 ± 2.9	6.7 ± 1.2	11 ± 4.5

By using the criteria described in Fig. 3, we counted the number of cells transfected with mt-GFP for each treatment group (15 or 30 μM for 0, 3, 6, 9 and 12 h), dividing them in "*normal*", "*mild*" or "*strong*" accordingly to the morphology they presented. A total number of 600 cells was counted in three independent experiments. The table presented data as percentage ± S.E. We compared the percentages of "normal", "mild" or "strong" classes from each treatment group with the respective classes in the control (e.g. no treatment; 0 h). The underlined values are significant accordingly to the *t*-test.

Table 2
ER morphology upon cadmium treatment

	15 μM cadmium treatment (h)				
	0	3	6	9	12
ER morphology description					
Normal	98 ± 1.1	97.83 ± 1.4	95.3 ± 1.8	81.2 ± 5	65.2 ± 7.4
Mild	1.5 ± 1.2	1.83 ± 1.8	3.5 ± 1.5	13.5 ± 3	24 ± 6.1
Strong	0.5 ± 0	0.34 ± 0.3	1.2 ± 1.2	5.3 ± 2.1	10.8 ± 2.6
	30 μM cadmium treatment (h)				
	0	3	6	9	12
ER morphology description					
Normal	96.33 ± 2	87.0 ± 3.2	82.8 ± 4	71.7 ± 11.2	57.2 ± 7.7
Mild	2.34 ± 2.1	8.3 ± 1.4	7.7 ± 2.1	20.1 ± 8.1	30.3 ± 3.3
Strong	1.33 ± 0.7	4.7 ± 1.8	9.5 ± 2.1	8.2 ± 3.2	12.5 ± 5

By using the criteria described in Fig. 4, we counted the number of cells transfected with ER-GFP for each treatment group (15 or 30 μM for 0, 3, 6, 9 and 12 h), dividing them in "*normal*", "*mild*" or "*strong*" accordingly to the morphology they presented. A total number of 600 cells was counted in three independent experiments. The table presents data as percentage ± S.E. We compared the percentages of "normal", "mild" or "strong" classes from each treatment group with the respective classes in the control (e.g. no treatment; 0 h). The underlined values are significant accordingly to the *t*-test.

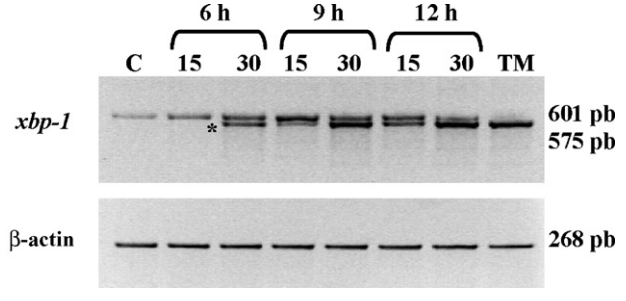

Fig. 5. *xbp-1* processing during cadmium treatment: RT-PCR analysis. The unspliced, normal form of *xbp-1* is shown as an amplicon of 601 bp. The 575 bp fragment associated to the spliced form of *xbp-1* is marked by an asterisk (*). The exposure to 10 μg/ml for 24 h of tunicamycin (TM) was used as positive control while β-actin was used as loading control.

spliced variant of *xbp-1* was clearly detectable in comparison to the unspliced 601 bp form.

3.4.2. Caspase-12 activation

To determine whether ER specific apoptotic pathway is involved in cadmium-induced cell death, we analysed the activation of pro-caspase-12 by immunoblotting experiments. Using a monoclonal antibody directed against pro-caspase-12 a single band corresponding to the p53 proform of caspase-12 was detected in control cells and – to a lower extent – in cadmium-treated fibroblasts (Fig. 6a and b). The antibody was only able to recognise the inactive proform of caspase-12, however, cadmium exposures (9–12 h; 15 μM $CdCl_2$) caused a significant decrease in the proform suggesting that caspase-12 had been cleaved and thus activated during cadmium-induced apoptosis (Fig. 6a).

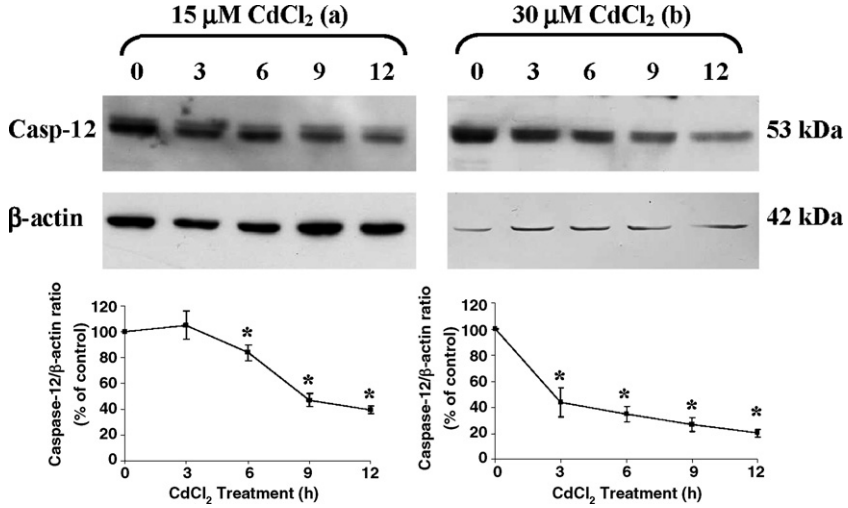

Fig. 6. Effects of cadmium-treatment on caspase-12 activation. Equal amount of total protein from cadmium treated and control cells were electrophoresed and anti-pro-caspase-12 antibody was used in WB experiments. A representative picture and a densitometric graph for each time course is presented: (a) 15 μM $CdCl_2$ and (b) 30 μM $CdCl_2$. β-actin was used as a loading control, reprobing the same membrane. The activation of caspase-12 (expressed as percentage of casp-12/β-actin) is presented as a black line. The asterisks indicate a significant difference for a defined treatment group in comparison to control ($p < 0.05$).

An earlier activation of caspase-12 was observed by using 30 μM $CdCl_2$ (6–12 h) as shown in Fig. 6b. These observations demonstrated that the cleavage of pro-caspase 12 correlated well with the induction of ER stress. β-actin was used as a loading control, reprobing the same membrane.

3.5. CytC release from mitochondria

To confirm the induction of mitochondrial stress during cadmium injury, we analysed the time course release of cytC from mitochondria to the cytosol (Fig. 7). We performed mitochondria fractionation using the voltage-

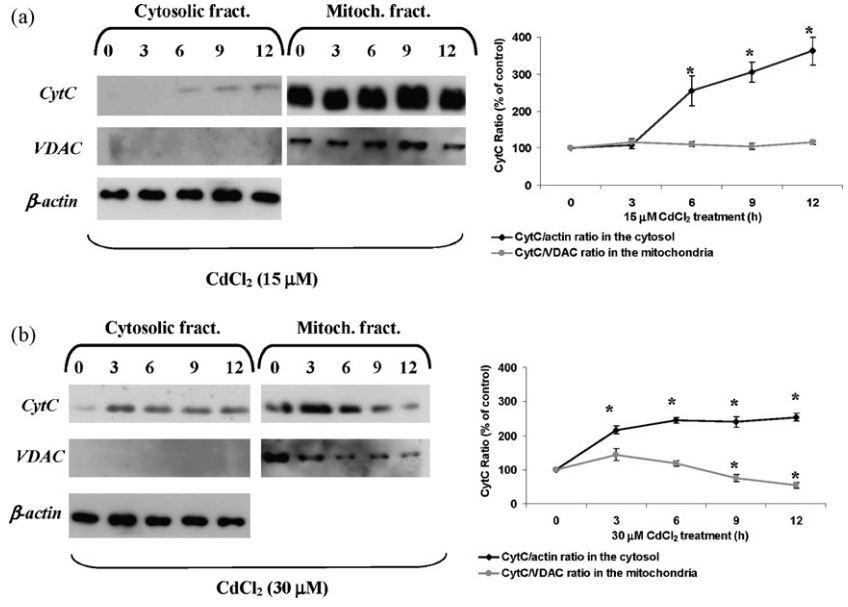

Fig. 7. Release of CytC from mitochondria: Western-blotting experiments. We performed mitochondrial fractionation of control and cadmium-treated with for different times (0, 3, 6, 9 and 12 h). Cytosolic and mitochondrial fractions of cell treated with 15 μM $CdCl_2$ (a) and 30 μM $CdCl_2$ (b) are presented. The quality of the fractionation was checked by using VDAC protein as mitochondrial marker in both cytosolic and mitochondrial fractions; β-actin was used as loading control for cytosolic fractions. A densitometric analysis for different cadmium treatments is presented in (a) and in (b) (15 and 30 μM, respectively). The release of CytC (expressed as percentage of CytC/β-actin) in the cytosolic fraction is presented as a black line; the CytC content (expressed as percentage of CytC/VDAC) in the mitochondrial fraction is presented in gray. The asterisks indicated a significant difference for a defined treatment group in comparison to control ($p < 0.05$).

dependent-anion-channel (VDAC) protein as mitochondrial marker to check the quality of the organelle fractionation and β-actin as loading control. The release of cytC in the cytosol of cadmium treated cells was dose and time dependent: using 15 μM of $CdCl_2$ we could observe a significant release of cytC after 6 h of treatment. The released quantity of cytC in the cytosol further increased following 9 and 12 h of cadmium treatment (Fig. 7a and graph). In parallel to mitochondrial morphology data, administration of the higher concentration of cadmium (30 μM) caused an earlier release of cytC (3 h) as reported in Fig. 7b. In this second set of experiments, a corresponding decrease of cytC in the mitochondrial fraction could be also observed following cadmium treatment.

4. Discussion

For the assessment of cadmium effects on cellular Ca^{2+} homeostasis we used the calcium-sensitive photoprotein, aequorin. Targeted AEQ chimeras have been employed successfully to measure organelle-specific modulation of Ca^{2+} homeostasis [36–38]. This method is a valuable alternative to the use of traditional Ca^{2+} fluorescent indicators, often criticized for their ability to bind cadmium with the same affinity of calcium [21]. To directly investigate the role of cadmium on Ca^{2+} homeostasis, we have selectively measured the Ca^{2+} concentration in different cell compartments, i.e., the cytoplasm and the organelles acting as sources (ER) or targets (mitochondria) of the Ca^{2+} signal. Effects of cadmium exposure on the cytosolic Ca^{2+} signal elicited by an agonist, bradykinin (Bk), have been investigated previously [40]; here we focused our attention on mitochondria and on the ER. Bk stimulation caused a rapid decrease in $[Ca^{+2}]_{ER}$ and a corresponding rise in mitochondrial Ca^{2+} concentration (and in cytosolic $[Ca^{2+}]$). In cadmium treated cells lower $[Ca^{2+}]_{ER}$ steady states were obtained and, consequently, the extent of Ca^{2+} release through IP_3-gated channels after Bk stimulation significantly declined. It is well known that the steady state Ca^{2+} concentration in the ER depends on the equilibrium between active accumulation and passive leak, and the effect of Cd^{2+} could be on either process. We investigated both possibilities independently and our results showed that cadmium significantly inhibited the activity of SERCAs, whereas no relevant effect was found on passive Ca^{2+} leakage from the ER.

Several studies demonstrated that strong modification in Ca^{2+} homeostasis could lead to ER-stress and, possibly, to cell death [27]: uncontrolled increases but also strong depletion in $[Ca^{2+}]_{ER}$, in fact, are known to trigger apoptotic cell death by direct activation of ER-resident caspase-12 [29]. In accordance with these reports, we observed that cadmium treatment caused an alteration in ER calcium homeostasis, thus leading to ER stress – activation of Ire1, processing *xbp-1*, disruption of ER morphology – and, finally, induction of apoptosis mediated by caspase-12.

Our data corroborated previous observations by Tchounwou et al. [45] and, more recently, Liu et al. [46], reporting the up-regulation of some ER chaperones (GADD/CHOP and Grp78, respectively) upon cadmium treatment. These proteins counteract the congestion of misfolded proteins intermediates during unbalance in the $[Ca^{2+}]_{ER}$ and ER stress, thus trying to promote cell survival. However, as a consequence of a prolonged or very severe stress, the activity of chaperones resulted inadequate and apoptotic cell death took place. To our knowledge this is the first report demonstrating that caspase-12 is activated in cadmium-induced apoptosis and highlighting the ER as a further cellular target of cadmium toxicity.

To understand which intracellular organelle could be most sensitive to cadmium toxicity, we performed time course experiments, with parallel analyses of effects on ER and mitochondria, well-known targets of cadmium toxicity. Previous findings, in fact, correlated mitochondrial dysfunctions with cadmium treatment [24,25]. Moreover, other laboratories described a decrease in rhodamine 123 fluorescence during cadmium-induced apoptosis in Rat-1 fibroblasts, suggesting that this heavy metal could act by altering the permeability and so the function of the mitochondrial membrane [47]. However, even if the role of mitochondria in cadmium-induced cell death is well characterized, the involvement of caspase-9 is discussed controversial by some authors [48–49]. In our hands, a strong modification in mitochondrial architecture was observed following cadmium treatment and the morphological changes were accompanied by a dose and time dependent release of CytC, linking acute cadmium toxicity with mitochondria mediated induction of cell death.

The parallel analysis of cadmium effects on ER and mitochondria, however, revealed a very complex pathway and comparable results were obtained for both the organelles. ER and mitochondria morphologies showed a synchronous pattern of structural and functional disruptions so that cytC release well correlated with ER stress and caspase-12 activation. The use of the higher cadmium concentration (30 μM), provided a more critical situation, but, even in this case, similar effects on these two organelles were observed. It seems that cadmium can exert a very complicated cascade of events into the cell and more than one distinct pathway can be activated following treatment.

In summary, we propose a "two hits" model for cadmium-induced apoptosis (Fig. 8). On one side, cadmium once entered the cell by receptor or voltage operated calcium channels, can directly or indirectly damages mitochondria, thus mediating cytC release and caspase-9 activation. On the other side, a novel analysis revealed ER as cellular target of cadmium toxicity. Cadmium-induced release of Ca^{2+} from ER stores (via stimulation of IP_3 gated channels, Fig. 8a) and cadmium-mediated inhibition of SERCA pumps are proposed to cause a generalized alteration of Ca^{2+} homeostasis – increase in $[Ca^{2+}]_{cyt}$ and prolonged reduction in $[Ca^{2+}]_{ER}$. The disruption in ER calcium homeostasis compromise the ER compartment, thus inducing ER stress and ER-mediated

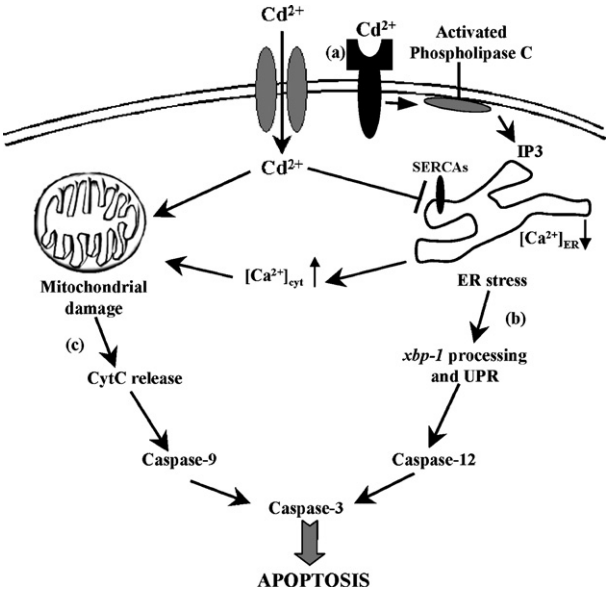

Fig. 8. Scheme of the proposed pathways mediating cadmium-induced apoptosis. Cadmium induces ER calcium release trough IP_3 pathway. Consequently, the cytosolic calcium concentration increases $[Ca^{2+}]_{cyt}$ (a) [20]. Cadmium, however, could also enter the cells through calcium channels and, once inside the cells, it causes SERCAs inhibition. Probably the concerted action of cadmium on SERCAs inhibition and IP_3 pathways is responsible for ER stress (*xbp-1* processing), UPR induction and finally caspase-12 activation (b). On the other hand cadmium provokes mitochondrial damage with inhibition of electron transport chain, R.O.S production, cytosolic release of pro-apoptotic factors (such as Cyt C), and finally activation of the caspase-9 (c). These two pathways seem to be contemporary activated and their parallel, synergic action promotes apoptosis.

apoptosis. Even if correlations between mitochondrial and ER stress pathways could not be ruled out, other studies will be necessary to complete this complex scenario.

Acknowledgements

We wish to thank Prof. Detmar Beyersmann (University of Bremen, Germany) for critical reading of the manuscript. We are grateful to Dr. Mercedes Garcia Gil (University of Pisa, Italy) for the precious gift of anti-caspase-12 antibody. We wish to thank Dr. Silvano Piazza (Laboratorio Nazionale CIB, Trieste, Italy) for helpful discussion with statistical analysis. We thank the Italian University Ministry (MURST), Telethon, Italy (grant nos. GGP05284 and GTF02013), the Italian Association for Cancer Research (AIRC), the Italian Space Agency (ASI), EU (fondi strutturali Obiettivo 2) and the PRRIITT program of the Emilia Romagna Region for financial support. M. Biagioli was recipient of a short-term fellowship by the Italian Association of Cellular and Developmental Biology (ABCD).

References

[1] World Health Organization (WHO), Cadmium. Environmental Health Criteria, vol. 135, WHO, Geneva, 1992.
[2] D. Beyersmann, S. Hechtenberg, Cadmium, gene regulation and cellular signalling in mammalian cells, Toxicol. Appl. Pharmacol. 144 (1997) 247–261.
[3] IARC, Monographs on the evaluation of carcinogenic risks to humans, vol. 58: Beryllium, Cadmium, Mercury, and Exposure in the Glass Manufacturing Industry, International Agency for Research on Cancer, Lyon, France, 1993.
[4] M.P. Waalkes, Cadmium carcinogenesis, Mutat. Res. 533 (2003) 107–120.
[5] J.D. Robertson, S. Orrenius, Molecular mechanisms of apoptosis induced by cytotoxic chemicals, Crit. Rev. Toxicol. 30 (2000) 609–627.
[6] M. Li, T. Kondo, Q.L. Zhao, F.J. Li, K. Tanabe, Y. Arai, Z.C. Zhou, M. Kasuya, Apoptosis induced by cadmium in human lymphoma U937 cells through Ca^{2+}-calpain and caspase-mitochondria-dependent pathways, J. Biol. Chem. 275 (2000) 39702–39709.
[7] M. Li, T. Xia, C.S. Jiang, L.J. Li, J.L. Fu, Z.C. Zhou, Cadmium directly induced the opening of membrane permeability pore of mitochondria which possibly involved in cadmium-triggered apoptosis, Toxicology 194 (2003) 19–33.
[8] M.J. Berridge, P. Lipp, M.D. Bootman, The versatility and universality of calcium signalling, Nat. Rev. Mol. Cell. Biol. 1 (2000) 11–21.
[9] M.P. Mattson, S.L. Chan, Calcium orchestrates apoptosis, Nat. Cell Biol. 5 (2003) 1041–1043.
[10] D. Ferrari, P. Pinton, G. Szabadkai, M. Chami, M. Campanella, T. Pozzan, R. Rizzuto, Endoplasmic reticulum, Bcl-2 and Ca(2+) handling in apoptosis, Cell Calcium 32 (2002) 413–420.
[11] R.D. Shannon, Revised effective ionic radii and systematic studies of Interatomic distances in halides and chalcogenides, Acta Cryst. A32 (1976) 751–767.
[12] T.J. McNulty, C.W. Taylor, Extracellular heavy-metal ions stimulate Ca^{2+} mobilization in hepatocytes, Biochem. J. 339 (1999) 555–561.
[13] C. Usai, A. Barberis, L. Moccagatta, C. Marchetti, Pathways of cadmium influx in mammalian neurons, J. Neurochem. 72 (1999) 2154–2161.
[14] T. Nasu, Effect of treatment time on calcium antagonism by cadmium ions in a guinea-pig taenia coli, J. Auton. Pharmacol. 19 (1999) 131–137.
[15] P.M. Verbost, G. Flik, P.K. Pang, R.A. Lock, S.E. Wendelaar Bonga, Cadmium inhibition of the erythrocyte Ca^{2+} pump. A molecular interpretation, J. Biol. Chem. 264 (1989) 5613–5615.
[16] P.M. Verbost, M.H. Senden, C.H. van Os, Nanomolar concentrations of Cd^{2+} inhibit Ca^{2+} transport systems in plasma membranes and intracellular Ca^{2+} stores in intestinal epithelium, Biochim. Biophys. Acta 902 (1987) 247–252.
[17] P.J. Vig, R. Nath, D. Desaiah, Metal inhibition of calmodulin activity in monkey brain, J. Appl. Toxicol. 9 (1989) 313–316.
[18] S. Hechtenberg, D. Beyersmann, Inhibition of sarcoplasmic reticulum Ca(2+)-ATPase activity by cadmium, lead and mercury, Enzyme 45 (1991) 109–115.
[19] G.H. Zhang, M. Yamaguchi, S. Kimura, S. Higham, N. Kraus-Friedmann, Effects of heavy metal on rat liver microsomal Ca^{2+}-ATPase and Ca^{2+} sequestrin, J. Biol. Chem. 265 (1990) 2184–2189.
[20] J.B. Smith, S.D. Dwyer, L. Smith, Cadmium evokes inositol polyphosphate formation and calcium mobilization, J. Biol. Chem. 264 (1989) 7115–7118.
[21] P.M. Hinkle, E.D. 2nd Shanshala, E.J. Nelson, Measurement of intracellular cadmium with fluorescent dyes, further evidence for the role of calcium channels in cadmium uptake, J. Biol. Chem. 267 (1992) 25553–25559.
[22] D.R. Green, J.C. Reed, Mitochondria and apoptosis, Science 281 (1998) 1309–1312.
[23] K.F. Ferri, G. Kroemer, Organelle-specific initiation of cell death pathways, Nat. Cell Biol. 3 (2001) E255–E263.
[24] W. Watjen, D. Beyersmann, Cadmium-induced apoptosis in C6 glioma cells: influence of oxidative stress, Biometals 17 (2004) 65–78.

[25] S.H. Oh, S.C. Lim, A rapid and transient ROS generation by cadmium triggers apoptosis via caspase-dependent pathway in HepG2 cells and this is inhibited through *N*-acetylcysteine-mediated catalase upregulation, Toxicol. Appl. Pharmacol. 212 (2006) 212–223.
[26] W. Watjen, H. Haase, M. Biagioli, D. Beyersmann, Induction of apoptosis in mammalian cells by cadmium and zinc, Environ. Health Perspect. 110 (2002) 865–867.
[27] C. Xu, B. Bailly-Maitre, J.C. Reed, Endoplasmic reticulum stress: cell life and death decisions, J. Clin. Invest. 115 (2005) 2656–2664.
[28] S. Orrenius, B. Zhivotovsky, P. Nicotera, Regulation of cell death: the calcium-apoptosis link, Nat. Rev. Mol. Cell Biol. 4 (2003) 552–565.
[29] T. Nakagawa, H. Zhu, N. Morishima, E. Li, J. Xu, B.A. Yanker, J. Yuan, Caspase-12 mediates endoplasmic-reticulum-specific apoptosis and cytotoxicity by amyloid-b, Nature 403 (2000) 98–103.
[30] M. Lamkanfi, M. Kalai, P. Vandenabeele, Caspase-12: an overview, Cell Death Differ. 11 (2004) 365–368.
[31] H. Yoshida, T. Matsui, A. Yamamoto, T. Okada, K. Mori, XBP1 mRNA is induced by ATF6 and spliced by IRE1 in response to ER stress to produce a highly active transcription factor, Cell 107 (2001) 881–891.
[32] M. Calfon, H. Zeng, F. Urano, J.H. Till, S.R. Hubbard, H.P. Harding, S.G. Clark, D. Ron, IRE1 couples endoplasmic reticulum load to secretory capacity by processing the XBP-1 mRNA, Nature 415 (2002) 92–96.
[33] A.H. Lee, N.N. Iwakoshi, L.H. Glimcher, XBP-1 regulates a subset of endoplasmic reticulum resident chaperone genes in the unfolded protein response, Mol. Cell Biol. 23 (2003) 7448–7459.
[34] M.M. Bradford, A rapid and sensitive method for the quantitation of microgram quantities of protein utilizing the principle of protein-dye binding, Anal. Biochem. 72 (1976) 248–254.
[35] J. Yang, X. Liu, K. Bhalla, C.N. Kim, A.M. Ibrado, J. Cai, T.I. Peng, D.P. Jones, X. Wang, Prevention of apoptosis by Bcl-2: release of cytochrome c from mitochondria blocked, Science 275 (1997) 1129–1132.
[36] A. Chiesa, E. Rapizzi, V. Tosello, P. Pinton, M. de Virgilio, K.E. Fogarty, R. Rizzuto, Recombinant aequorin and green fluorescent protein as valuable tools in the study of cell signalling, Biochem. J. 355 (2001) 1–12.
[37] M. Montero, M.J. Barrero, J. Alvarez, [Ca^{2+}] microdomains control agonist-induced Ca^{2+} release in intact HeLa cells, FASEB J. 11 (1997) 881–885.
[38] M.J. Barrero, M. Montero, J. Alvarez, Dynamics of [Ca^{2+}] in the endoplasmic reticulum and cytoplasm of intact HeLa cells. A comparative study, J. Biol. Chem. 272 (1997) 27694–27699.
[39] P. Pinton, T. Pozzan, R. Rizzuto, The Golgi apparatus is an inositol 1,4,5-trisphosphate-sensitive Ca^{2+} store, with functional properties distinct from those of the endoplasmic reticulum, EMBO J. 17 (1998) 5298–5308.
[40] R. Rizzuto, P. Pinton, W. Carrington, F.S. Fay, K.E. Fogarty, L.M. Lifshitz, R.A. Tuft, T. Pozzan, Close contacts with the endoplasmic reticulum as determinants of mitochondrial Ca^{2+} responses, Science 280 (1998) 1763–1766.
[41] Y. Okano, T. Fu, Y. Nozawa, Calcium oscillation induced by bradykinin in polyoma middle T antigen-transformed NIH3T3 fibroblasts: evidence for dependence on protein kinase C, Biochem. Biophys. Res. Commun. 176 (1991) 813–819.
[42] M. Biagioli, P. Pinton, R. Scudiero, M. Ragghianti, S. Bucci, R. Rizzuto, Aequorin chimeras as valuable tool in the measurement of Ca^{2+} concentration during cadmium injury, Toxicology 208 (2005) 389–398.
[43] P. Pinton, S. Leo, M.R. Wieckowski, G. Di Benedetto, R. Rizzuto, Long-term modulation of mitochondrial Ca^{2+} signals by protein kinase C isozymes, J. Cell Biol. 165 (2004) 223–232.
[44] P. Pinton, D. Ferrari, P. Magalhaes, K. Schulze-Osthoff, F. Di Virgilio, T. Pozzan, R. Rizzuto, Reduced loading of intracellular Ca(2+) stores and downregulation of capacitative Ca(2+) influx in Bcl-2-overexpressing cells, J. Cell Biol. 148 (2000).
[45] P.B. Tchounwou, A.B. Ishaque, J. Schneider, Cytotoxicity and transcriptional activation of stress genes in human liver carcinoma cells (HepG2) exposed to cadmium chloride, Mol. Cell Biochem. 222 (2001) 21–28.
[46] F. Liu, K. Inageda, G. Nishitai, M. Matsuoka, Cadmium induces the expression of Grp78, an endoplasmic reticulum molecular chaperone, in LLC-PK1 renal epithelial cells, Environ. Health Perspect. 114 (2006) 859–864.
[47] M.S. Kim, B.J. Kim, H.N. Woo, K.W. Kim, K.B. Kim, I.K. Kim, Y.K. Jung, Cadmium induces caspase-mediated cell death: suppression by Bcl-2, Toxicology 145 (2000) 27–37.
[48] M. Kondoh, S. Araragi, K. Sato, M. Higashimoto, M. Takiguchi, M. Sato, Cadmium induces apoptosis partly via caspase-9 activation in HL-60 cells, Toxicology 170 (2002) 111–117.
[49] H.Y. Shih, C.J. Lin, S.W. Hsu, S.H. Wang, W.L. Chen, M.T. Lee, Y.H. Wei, C.M. Shih, Cadmium toxicity toward caspase-independent apoptosis through the mitochondria-calcium pathway in mtDNA-depleted cells, Ann. NY. Acad. Sci. 1042 (2005) 497–505.